

# On the Robustness of RSMA to Adversarial BD-RIS-Induced Interference

Arthur S. de Sena, *Member, IEEE*, Jacek Kibilda, *Senior Member, IEEE*, Nurul H. Mahmood, *Member, IEEE*, André Gomes, *Member, IEEE*, Luiz A. DaSilva, *Fellow, IEEE*, Matti Latva-aho, *Fellow, IEEE*

**Abstract**—This article investigates the robustness of rate-splitting multiple access (RSMA) in multi-user multiple-input multiple-output (MIMO) systems to interference attacks against channel acquisition induced by beyond-diagonal RISs (BD-RISs). Two primary attack strategies, random and aligned interference, are proposed for fully connected and group-connected BD-RIS architectures. Valid random reflection coefficients are generated exploiting the Takagi factorization, while potent aligned interference attacks are achieved through optimization strategies based on a quadratically constrained quadratic program (QCQP) reformulation followed by projections onto the unitary manifold. Our numerical findings reveal that, when perfect channel state information (CSI) is available, RSMA behaves similarly to space-division multiple access (SDMA) and thus is highly susceptible to the attack, with BD-RIS inducing severe performance loss and significantly outperforming diagonal RIS. However, under imperfect CSI, RSMA consistently demonstrates significantly greater robustness than SDMA, particularly as the system's transmit power increases.

**Index Terms**—Reconfigurable intelligent surface, rate-splitting multiple access, physical-layer security, multi-user MIMO.

## I. INTRODUCTION

6G introduces a range of new technologies that will positively contribute to improved service and feature offerings at the expense of greatly expanding the threat surface. Reconfigurable intelligent surface (RIS) is one example of a benign technology that is anticipated to contribute to improved coverage, spectral efficiency, and sensing services, but one that has also attracted significant interest in the adversarial context [1]–[8]. Being a passive relay, RIS can be used as a passive jammer that can adjust its reflective properties to execute an adversarial action, e.g., canceling the legitimate signal [1], aiding the active jammer [2], or poisoning the channel estimation process [3]. The latter attack is of particular severity, since channel acquisition is a critical component of advanced wireless communication systems that rely on multiple-input multiple-output (MIMO) technology. Here, space-division multiple access (SDMA), in particular, has been shown to be susceptible to a RIS-induced attack that requires no or limited channel state information (CSI) [5]–[8]. However, not all MIMO multiple access protocols are equally vulnerable. Specifically, in our preliminary work on rate-splitting multiple access (RSMA) [9], we observed a

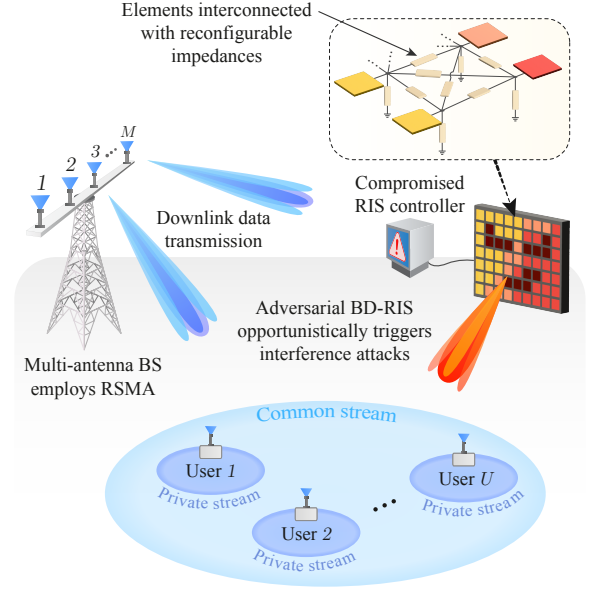


Fig. 1: An adversarial entity configures a BD-RIS to launch interference attacks on multiple RSMA users during downlink data transmission.

surprising robustness of RSMA to RIS-induced attacks under imperfect CSI.

RSMA is a split transmission scheme whereby the base station (BS) encodes a part of the users' data into private messages - transmitted via private precoders - with the remaining users' data being encoded into a common message - transmitted via a common precoder [10], [11]. On the receiver side, successive interference cancellation (SIC) is utilized to aid in decoding the individual users' messages. The private precoders are designed as unicast precoders, which - similarly to SDMA - makes them sensitive to imperfect CSI. The common precoder is constructed as a multicast precoder and, thus, should be more robust to inter-user interference arising due to CSI imperfections. Consequently, by adaptively re-allocating the power between the private and common precoders, RSMA is able to adapt to CSI imperfection [11]. However, the full extent of RSMA's susceptibility to mismatched CSI due to RIS-induced attacks is not yet completely understood. In particular, novel RIS architectures that feature non-diagonal reflection matrices have been proposed recently. These architectures, referred to as beyond-diagonal

Arthur S. de Sena, Nurul H. Mahmood, and Matti Latva-aho are with the University of Oulu, Oulu, Finland (email: arthur.sena@oulu.fi, nurul-huda.mahmood@oulu.fi, matti.latva-aho@oulu.fi).

Jacek Kibilda and Luiz DaSilva are with the Commonwealth Cyber Initiative, Virginia Tech, USA (email: jkibilda@vt.edu, ldasilva@vt.edu).

André Gomes is with Rowan University, USA (email: gomesa@rowan.edu).

RISs (BD-RISs), generalize conventional RIS designs by introducing inter-element connections [12]. Such connections enable more advanced optimization capabilities and enhanced energy radiation, which in turn boosts reflection performance at the cost of additional circuit complexity. Nevertheless, the enhanced reflection efficiency of BD-RISs may also strengthen their adversarial capabilities, potentially leading to attacks with increased degradation impact. Identifying the distinct vulnerabilities that BD-RISs may introduce to RSMA systems and the advantages that would motivate an attacker to leverage BD-RISs constitutes a major research gap.

This article reports on our extensive study and analysis of the robustness of the RSMA protocol to attacks against channel acquisition induced by BD-RISs. In our study, we consider three BD-RIS element network architectures: *fully connected*, *group-connected*, and *single-connected* (corresponding to the diagonal RIS). For each architecture, we propose two different BD-RIS-induced interference attacks that exploit the training protocol employed at the BS, namely *random* and *aligned*. In both attacks, during uplink pilot training, the BD-RIS is configured to absorb or reflect with random reflection coefficients. Then, during data transmission, the BD-RIS is configured with newly generated random reflection coefficients (random attack) or with optimized coefficients that maximize the reflected power based on the knowledge of the RIS channels (aligned attack). In each case, the proposed algorithm finds a set of reflection coefficients that satisfy the symmetry and unitary constraints of the BD-RIS.

Our numerical study reveals that, when perfect CSI is available, RSMA behaves similarly to SDMA and thus is highly susceptible to the attack, with BD-RIS group-connected and fully connected architectures inducing larger performance degradations than a single-connected RIS. However, RSMA displays a surprising degree of robustness to the BD-RIS-induced attack when the CSI is imperfect, as we have reported in our conference paper [9]. When the system is under the BD-RIS-induced attack, the adaptation mechanism of RSMA reacts to the inaccurate CSI by allocating more power to the common message. When the transmit power is low (below 10 dBm) RSMA's rate is being severely degraded by the attack (on par with SDMA), but as the transmit power increases, RSMA is able to recover from the attack. This trend can be observed across all types of BD-RIS attacks. In order to directly quantify this inherent robustness, we propose the *robustness index* that we define and discuss in subsequent sections. Interestingly, when we gradually adjust the CSI error, the robustness index for SDMA steadily decreases. In contrast, RSMA's robustness index shows a local maximum, as it increases with lower values of CSI error, followed by a slow decline, although remaining significantly above SDMA's robustness. This highlights the ability of RSMA to sustain performance under attack, especially in environments with low to moderate channel errors. When the CSI of channels adjacent to the RIS varies, the architecture of the RIS exploited by the attacker becomes a relevant factor, even when the optimization driving the attack is based on erroneous channel information. Our key contributions are as follows:

- We propose and analyze two distinct attack strategies,

employing either random or optimized reflection coefficients, for each BD-RIS architecture. These strategies are designed to rigorously satisfy the inherent constraints of the respective BD-RIS types, and are targeted at disrupting multi-user data transmission in an RSMA system.

- For the random interference attack strategy, we leverage matrix theory to develop a simple algorithm based on Takagi factorization. This algorithm generates valid random BD-RIS reflection coefficient matrices that are symmetric and unitary (or block-wise symmetric and unitary for group-connected BD-RIS architectures).
- For the aligned interference attack strategy, we propose an algorithm to maximize the unwanted reflected power towards legitimate users. To address the resulting complex optimization problems, we exploit the symmetric structure of the BD-RIS reflection matrices by employing duplication matrices. This approach reformulates the problems into simplified quadratically constrained quadratic program (QCQP) versions that are efficiently solvable using singular value decomposition (SVD), followed by projections onto the unitary manifold via the Takagi factorization.
- We propose and thoroughly investigate two metrics to quantify the robustness of RSMA systems against BD-RIS-induced attacks: rate degradation and a robustness index, ranging from 0 (minimum robustness) to 1 (full robustness). Our findings demonstrate that under imperfect CSI, RSMA exhibits substantially greater robustness compared to non-adaptive protocols such as SDMA. For instance, under aligned interference attacks induced by a sufficiently large fully connected RIS, RSMA can achieve a robustness index of nearly 0.7, while SDMA's falls below 0.5 under similar conditions.
- Furthermore, we reveal that BD-RIS offers a significant adversarial advantage over conventional RIS across all investigated scenarios, both under random and aligned interference attacks, an advantage that becomes particularly pronounced when the attacking RIS operates in a reflective mode during the uplink pilot training phase, leading to a significant decrease in the system sum rate.

*Notation:* Boldface lower-case letters denote vectors and upper-case represent matrices. The  $\ell_2$  norm of a vector  $\mathbf{a}$  is denoted by  $\|\mathbf{a}\|_2$ , and the Frobenius norm of a matrix  $\mathbf{A}$  by  $\|\mathbf{A}\|_F$ . The  $i$ th column of a matrix  $\mathbf{A}$  is denoted by  $[\mathbf{A}]_{:,i}$ , the transpose and Hermitian transpose of  $\mathbf{A}$  are represented by  $\mathbf{A}^T$  and  $\mathbf{A}^H$ , respectively, and  $\otimes$  represents the Kronecker product. The operator  $\text{vec}(\cdot)$  transforms a matrix into a column vector by stacking its columns sequentially,  $\text{unvec}(\cdot)$  reshapes a vectorized matrix into its original dimensions, and  $\text{vech}(\cdot)$  is the half-vectorization operator, which stacks the elements from the lower triangular part (including the main diagonal) of a square matrix into a column vector. Moreover,  $\text{vecd}(\cdot)$  converts the diagonal elements of a square matrix into a column vector,  $\text{diag}(\cdot)$  transforms a vector into a diagonal matrix, and  $\text{bdiag}(\cdot)$  constructs a block diagonal matrix sequentially formed by the input matrices.

## II. RELATED WORK

The concept of an adversary that configures RIS to launch attacks against the wireless link was originally proposed in [1]. The proposed attack relied on using the RIS to create cancellation signals. Although the attack has the potential to cause significant power degradation in the receiver, the attack requires highly accurate CSI, which would limit its feasibility. Notably, many works that followed showed that a RIS-induced attack can be made effective with limited or even no CSI, as long as it takes advantage of the fact that for many wireless protocols the CSI acquisition is sufficiently separated in time from data transmission. For instance, in [3], it was shown that the channel equalization can be disrupted by the operation of the adversarial RIS that randomly flips its reflection pattern between channel acquisition and symbol transmission. This random flipping is particularly harmful to multiple access methods that rely on multi-user MIMO, such as SDMA. In this case, adversarial RIS increases CSI inaccuracy, making linear precoders ineffective in removing inter-user interference. Exactly this kind of attack with randomly set RIS coefficients, humorously referred to by their authors as the “disco-ball attack”, was proposed in [5], [13]. The optimized version of this attack that aligns the RIS channels to boost interference was proposed and studied in [6], [8]. Other protocols and services, such as beam management [14], physical layer key generation [15], [16], and integrated sensing and communication [17], [18], have also been shown to be vulnerable to the attack with RIS flipping its coefficients between different phases of the wireless protocol. However, many open questions remain in studying RIS-induced attacks, particularly as they relate to identifying protocols and methods that may be robust or resilient to the proposed attacks.

RSMA was introduced as a multiple access strategy that exploits a split transmission mechanism to adaptively treat inter-user interference at either the BS or receiver side, depending on the accuracy of the available CSI [10], [11]. When CSI is perfect, RSMA resorts to linear precoding at the BS that can effectively take care of the inter-user interference. On the other hand, when CSI is inaccurate, RSMA employs multicast transmission and SIC at the receiver side to decode (part of) inter-user interference. There are a variety of benefits that come from this increased flexibility, such as increased spectral and energy efficiency [19], improved outage [20], and reduced latency [21], [22]. RSMA has also been shown to be robust and resilient to user mobility [23], and binary link failures [24]. However, one of the properties gaining the most attention is its inherent robustness and resilience to inaccurate CSI [11], which can also be quantified, following [24]. Since RIS-induced interference attacks inherently rely on manipulating the CSI, the outstanding question is how robust RSMA is to inaccurate CSI that results from adversarial RIS activities.

In the preliminary work described in the conference version of this article, we considered the impact of adversarial RIS on RSMA [9]. What we observed is the surprising robustness of RSMA to the RIS-induced attack, which manifests itself under imperfect CSI scenarios. In this article, we extend our preliminary study by directly quantifying the robustness of

RSMA to adversarial attacks using a new metric that we refer to as the robustness index. We focus our attention on the impact of an attack with a BD-RIS architecture that generalizes conventional (diagonal) RIS. Alternative RIS architectures were considered for adversarial attacks to create non-reciprocal channels [25], and increase their angular span [26]. However, this is the first work that considers BD-RIS and inter-element connections in the context of an adversarial scenario. Consequently, in this paper, we propose a set of new algorithms that find valid reflection coefficients that obey the properties of BD-RIS. Furthermore, we consider different attack modes during the uplink pilot training, and the impact of adaptive power allocation, and SIC imperfections.

## III. SYSTEM MODEL

Consider the multi-user MIMO system depicted in Fig. 1, where a BS equipped with a linear array of  $M$  antennas communicates with  $U$  single-antenna users, represented by the index set  $\mathcal{U} = \{1, 2, \dots, U\}$ , with the aid of RSMA. The system operates in the presence of an adversarial entity that controls a BD-RIS comprising  $D$  reflecting elements. The attacker manipulates the BD-RIS to disrupt the channel estimation phase at the BS, configuring it to either absorb incoming pilots [5], [6] (absorption mode) or reflect them randomly [13] (reflective mode). The impact of the mode choice will be investigated in Section V.

Regardless of the RIS’s configuration during uplink training, the attacker generates a new set of reflecting coefficients during the data transmission phase, altering the propagation environment in a manner unknown to the BS. This ensures that the BS operates with corrupted CSI, as its estimates from the training phase do not reflect the RIS’s true, active configuration during data transmission. The discrepancy between estimated and actual CSI reduces the performance of precoders, ultimately generating inter-user interference. Fig. 2 illustrates the overall adversarial protocol.

### A. BD-RIS Architectures

We consider two BD-RIS types, the fully connected and group-connected architectures. In the fully connected BD-RIS, all elements are interconnected through reconfigurable impedances. A fully connected BD-RIS with  $D$  reflecting elements operates as a  $D$ -port reciprocal network. The interaction among elements is captured by the scattering matrix  $\Theta \in \mathbb{C}^{D \times D}$ , which characterizes the reflection behavior of the system. Energy conservation imposes the constraint  $\Theta\Theta^H \preceq \mathbf{I}_D$ , implying that the Frobenius norm satisfies  $\frac{1}{\sqrt{D}}\|\Theta\|_F \leq 1$ . When the circuit is lossless, the scattering matrix becomes unitary, i.e.,  $\Theta\Theta^H = \mathbf{I}_D$ . Furthermore, due to the reciprocal nature of the BD-RIS hardware, the symmetry condition  $\Theta = \Theta^T$  must also be satisfied. This property implies that  $\frac{D(D+1)}{2}$  independent coefficients are needed to fully define the entries of  $\Theta$ .

The group-connected architecture introduces a balance between complexity and performance. In this setup, the reflecting elements are divided into  $G$  independent groups, each of which

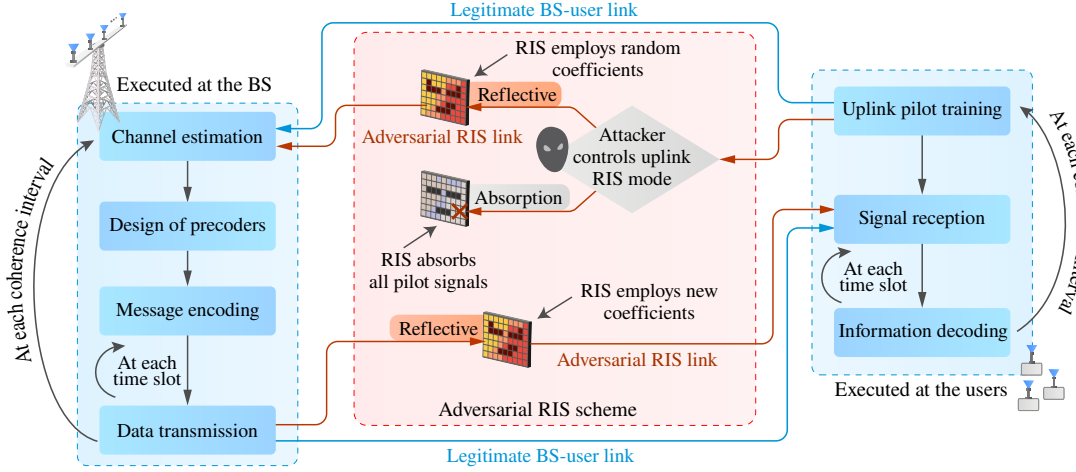


Fig. 2: Simplified diagram of the RIS-induced attack strategy.

forms a fully connected subnetwork. As a result, the overall scattering matrix exhibits a block diagonal structure:

$$\Theta = \text{bdiag}(\Theta_1, \dots, \Theta_G) \in \mathbb{C}^{D \times D}, \quad (1)$$

where each submatrix  $\Theta_g \in \mathbb{C}^{D_g \times D_g}$  models the signal reflections induced by its corresponding fully connected group, with  $D_g$  denoting the number of elements of the  $g$ th group, such that  $D = \sum_g D_g$ . Similar to the fully connected case, each submatrix satisfies the conditions  $\Theta_g = \Theta_g^T$  and  $\Theta_g \Theta_g^H \preceq \mathbf{I}_{D_g}$ . The number of independent parameters needed to configure each group is, therefore,  $\frac{D_g(D_g+1)}{2}$ , in which  $D_g \leq D$ . From this point onward, we consider lossless reflection models, i.e., we assume  $\Theta \Theta^H = \mathbf{I}_D$  and  $\Theta_g \Theta_g^H = \mathbf{I}_{D_g}$  for the fully and group-connected RIS, respectively. The impact of different adversarial strategies is analyzed in the following sections.

### B. RSMA Protocol

In RSMA, the BS partitions each user's message into common and private parts. Then, all common parts are encoded into a single symbol  $s^c$ , while each private part, intended for a specific user  $u$ , is modulated into a private symbol  $s_u^p$ .

Next, based on the acquired CSI, the BS designs two linear precoders:  $\mathbf{w}^c \in \mathbb{C}^M$  to deliver the common symbol  $s^c$  to all users and  $\mathbf{w}_u^p \in \mathbb{C}^M$  to transmit the private symbol  $s_u^p$  to its intended user. Finally, the precoded symbols are superimposed in the power domain, resulting in the transmitted signal:

$$\mathbf{s} = \mathbf{w}^c \sqrt{P\alpha^c} s^c + \sum_{i \in \mathcal{U}} \mathbf{w}_i^p \sqrt{P\alpha_i^p} s_u^p \in \mathbb{C}^M, \quad (2)$$

where  $\alpha^c$  and  $\alpha_i^p$  are the power coefficients for the common and private symbols, respectively, satisfying  $\alpha^c + \sum_{i \in \mathcal{U}} \alpha_i^p = 1$ , with  $P$  denoting the total transmission power. Users receive the superimposed data streams through both the direct link and the adversarial BD-RIS reflections. Thus, the received signal at user  $u$  is given by:

$$r_u = \mathbf{g}_u^H \Theta \mathbf{G} \mathbf{s} + \mathbf{h}_u^H \mathbf{s} + n_u, \quad (3)$$

where  $\mathbf{h}_u \in \mathbb{C}^M$ ,  $\mathbf{G} \in \mathbb{C}^{D \times M}$ , and  $\mathbf{g}_u \in \mathbb{C}^D$  model the propagation channels for the direct BS-user link, the BS-RIS link, and the RIS-user link, respectively, and  $n_u \in \mathbb{C}$  denotes the additive white Gaussian noise with variance  $\sigma^2$ .

Each user first decodes the common message, while treating all private signals as interference. Consequently, the signal-to-interference-plus-noise ratio (SINR) for the common message at user  $u$  is:

$$\gamma_u^c = \frac{|(\mathbf{g}_u^H \Theta \mathbf{G} + \mathbf{h}_u^H) \mathbf{w}^c|^2 P \alpha^c}{\sum_{i \in \mathcal{U}} |(\mathbf{g}_u^H \Theta \mathbf{G} + \mathbf{h}_u^H) \mathbf{w}_i^p|^2 P \alpha_i^p + \sigma^2}. \quad (4)$$

Since all users must successfully decode the common message, the corresponding achievable rate is dictated by the weakest user, resulting in:

$$R^c = \min_{u \in \mathcal{U}} R_u^c, \quad \text{where } R_u^c = \log_2(1 + \gamma_u^c). \quad (5)$$

Once the common message is recovered, SIC is applied to remove its contribution from  $r_u$ . Thus, the private SINR at user  $u$  is given by:

$$\gamma_u^p = \frac{|(\mathbf{g}_u^H \Theta \mathbf{G} + \mathbf{h}_u^H) \mathbf{w}_u^p|^2 P \alpha_u^p}{\sum_{i \in \mathcal{U}, i \neq u} |(\mathbf{g}_u^H \Theta \mathbf{G} + \mathbf{h}_u^H) \mathbf{w}_i^p|^2 P \alpha_i^p + \sigma^2}. \quad (6)$$

The achievable private rate at user  $u$  is then:

$$R_u^p = \log_2(1 + \gamma_u^p), \quad (7)$$

yielding a system sum rate of:

$$R = R^c + \sum_{i \in \mathcal{U}} R_i^p. \quad (8)$$

### C. Quantifying Robustness of RSMA

We propose two performance metrics to evaluate the robustness of RSMA against RIS-induced attacks, namely *rate degradation* and *robustness index*. The rate degradation quantifies the performance loss caused by an attack, computed as the difference between the baseline performance in a secure environment and the degraded performance during an attack. To this end, the common rate is assumed to be uniformly allocated among the users, i.e.,  $R^c/U$ . The overall effective

rate for user  $u$  is then the sum of this portion of the common rate and the individual private rate  $R_u^p$ . The rate degradation experienced by the  $u$ th user is defined as

$$\Delta R_u = \bar{R}_u^p - \tilde{R}_u^p + \frac{\bar{R}^c - \tilde{R}^c}{U}, \quad (9)$$

where  $\tilde{R}_u^p$  and  $\tilde{R}^c$  are the private and common rates observed when the system is under attack, and  $\bar{R}_u^p$  and  $\bar{R}^c$  are the reference rates in the absence of the attack.

The robustness index  $\kappa$  complements the rate degradation metric by evaluating the proportion of baseline performance retained during an attack. This normalized metric quantifies the system's ability to maintain performance under RIS-induced attacks relative to its baseline rates  $\bar{R}_u^p$  and  $\bar{R}^c$ . The robustness index is defined as

$$\kappa = \frac{1}{U} \sum_{u=1}^U \left( 1 - \frac{\Delta R_u}{\frac{\bar{R}^c}{U} + \bar{R}_u^p} \right). \quad (10)$$

Note that a higher degradation  $\Delta R_u$  leads to a lower robustness index  $\kappa \in [0, 1]$ , such that  $\kappa = 0$  indicates complete collapse, while  $\kappa = 1$  corresponds to complete robustness.

#### D. CSI Acquisition

Under the assumption of reciprocity, the downlink channels can be estimated at the BS based on uplink measurements from pilot signals transmitted by the users. As explained, during this phase, the attacker can configure the BD-RIS to either absorb or randomly reflect incoming signals. In absorption mode, the pilot signals impinging on the BD-RIS are prevented from reaching the BS. In the random reflective mode, on the other hand, the pilot signals will characterize the BD-RIS-related propagation paths. However, the attacker reconfigures the reflection coefficients in the data transmission phase, making the acquired CSI inaccurate. Thus, in both modes, only imperfect estimates of the channels  $\mathbf{h}_u$  are accessible to the BS. Adding to the BD-RIS disruptions, other rapid changes in the propagation environment and hardware limitations can also introduce errors in the estimation process. As a result, the direct link estimates will be a combination of the true channels and error components, modeled as:

$$\hat{\mathbf{h}}_u = \sqrt{1 - \varepsilon^{\text{BS-U}}} (\mathbf{h}_u + \psi \mathbf{G}^H \mathbf{\Theta} \mathbf{g}_u) + \sqrt{\varepsilon^{\text{BS-U}}} \mathbf{e}_u^{\text{BS-U}}, \quad (11)$$

where  $\hat{\mathbf{h}}_u \in \mathbb{C}^M$  is the estimated channel,  $\mathbf{e}_u^{\text{BS-U}} \in \mathbb{C}^M$  is a standard complex Gaussian error vector,  $\psi$  is a binary coefficient modeling the operation mode of the BD-RIS, with  $\psi = 0$  corresponding to absorption mode, and  $\psi = 1$  corresponding to reflective mode, and  $\varepsilon^{\text{BS-U}} \in [0, 1]$  is the error factor for the BS-user link. This model indicates that when  $\varepsilon^{\text{BS-U}} = 0$ , the channel estimate is perfect (i.e.,  $\hat{\mathbf{h}}_u = \mathbf{h}_u + \psi \mathbf{G}^H \mathbf{\Theta} \mathbf{g}_u$ ), while increasing values of  $\varepsilon^{\text{BS-U}}$  imply a larger error component in the estimate. Similarly, when  $\psi = 1$ , the uplink CSI is further perturbed by the adversarial BD-RIS link.

As for the attacker, we assume that it can only estimate the channels associated with its BD-RIS, also modeled as imperfect. Specifically, the estimates of the BS-RIS channel matrix and the RIS-user channel vector are given by

$$\hat{\mathbf{G}} = \sqrt{1 - \varepsilon^{\text{BS-RIS}}} \mathbf{G} + \sqrt{\varepsilon^{\text{BS-RIS}}} \mathbf{E}^{\text{BS-RIS}}, \quad (12)$$

and

$$\hat{\mathbf{g}}_u = \sqrt{1 - \varepsilon^{\text{RIS-U}}} \mathbf{g}_u + \sqrt{\varepsilon^{\text{RIS-U}}} \mathbf{e}_u^{\text{RIS-U}}, \quad (13)$$

where  $\mathbf{E}^{\text{BS-RIS}}$  and  $\mathbf{e}_u^{\text{RIS-U}}$  are the corresponding complex Gaussian error components, with  $\varepsilon^{\text{BS-RIS}}$  and  $\varepsilon^{\text{RIS-U}}$  denoting the error factors for the BS-RIS and RIS-user links, respectively.

#### E. BS Precoder Design

The private precoder should ensure that the interference observed at user  $u$  due to transmissions intended for any other user  $u'$  is negligible, i.e.,  $\mathbf{h}_u^H \mathbf{w}_u^p \approx 0, \forall u' \neq u$ . This objective is achieved via a regularized zero-forcing approach, which effectively mitigates inter-user interference while balancing noise enhancement. Specifically, the BS first constructs the estimated direct-link channel matrix as

$$\hat{\mathbf{H}} = [\hat{\mathbf{h}}_1, \hat{\mathbf{h}}_2, \dots, \hat{\mathbf{h}}_U] \in \mathbb{C}^{M \times U}. \quad (14)$$

Then, assuming that  $M \geq U$ , which guarantees that  $\hat{\mathbf{H}}$  has full column rank, the regularized zero-forcing precoding matrix can be computed as

$$\mathbf{W}^p = \hat{\mathbf{H}} \left( \hat{\mathbf{H}}^H \hat{\mathbf{H}} + \omega \mathbf{I} \right)^{-1} \in \mathbb{C}^{M \times U}, \quad (15)$$

where the regularization factor is given by  $\omega = \sigma^2/P$ . The private precoder for user  $u$  can be readily obtained by

$$\mathbf{w}_u^p = \beta_u^p [\mathbf{W}^p]_{:,u}, \quad (16)$$

where  $\beta_u^p = \frac{1}{(\mathbf{w}_u^p)^H \mathbf{w}_u^p}$  is the normalization factor for user  $u$ .

The common precoder  $\mathbf{w}^c$  should reliably deliver the common message across all users. However, its optimal design is NP-hard, while approximate solutions typically require iterative methods with high computational complexity [27]. To tackle this challenge, we adopt a low-complexity weighted matched filter (MF) approach as follows:

$$\mathbf{w}^c = \beta^c \sum_{i \in \mathcal{U}} v_i \hat{\mathbf{h}}_i, \quad (17)$$

where the normalization factor  $\beta^c = \left\| \sum_{i \in \mathcal{U}} v_i \hat{\mathbf{h}}_i \right\|_2^{-1}$  guarantees that  $\|\mathbf{w}^c\|_2 = 1$ , and  $v_i$  is the weight for the  $i$ th user. In particular, we prioritize users with weaker channel conditions by setting  $v_i = 1/\|\hat{\mathbf{h}}_i\|_2^2$ . This strategy ensures that users experiencing weaker channels receive higher priority in the common precoder design.

#### F. Power Allocation

The BS employs a power allocation policy aiming at the maximization of the system sum rate. Given the precoders  $\mathbf{w}^c$  and  $\mathbf{w}_u^p$  for each user  $u \in \mathcal{U}$ , the BS aims to solve the following optimization problem:

$$\max_{\alpha^c, \{\alpha_u^p\}_{u \in \mathcal{U}}} R^c + \sum_{u \in \mathcal{U}} R_u^p, \quad (18a)$$

$$\text{s.t.} \quad \alpha^c + \sum_{u \in \mathcal{U}} \alpha_u^p = 1, \quad (18b)$$

$$\alpha_u^p \geq 0, \quad \alpha^c \geq 0. \quad (18c)$$

A closed-form optimal solution for (18) is not possible due to the minimum operator in the common rate in (5), i.e.,  $R^c = \min_{u \in \mathcal{U}} R_u^c$ , and the coupled power coefficients, which make the problem non-convex. Instead, we propose a simple but effective approach to approximate our objective.

A meaningful way to perform power allocation is to keep the interference resulting from imperfect CSI approximately at the same level as the noise variance [11]. By doing this, the degradation of users' data rates can be mitigated. Mathematically, we aim to ensure in the SINR expression for the private stream,  $\gamma_u^p$ , that the interference term  $\sum_{i \neq u} |\mathbf{h}_u^H \mathbf{w}_i^p|^2 P \alpha^p \approx \sigma^2$ . To achieve this goal, we first adopt a uniform power allocation across the private messages, i.e.,  $\alpha^p = \alpha_u^p, \forall u \in \mathcal{U}$ . Then, it becomes clear that the desired  $\alpha^p$  should be inversely proportional to the private inter-user interference  $\sum_{i \neq u} |\mathbf{h}_u^H \mathbf{w}_i^p|^2 P$ . More specifically, for the  $u$ th user, we should have:

$$\sum_{i \neq u} |\mathbf{h}_u^H \mathbf{w}_i^p|^2 P \alpha^p \approx \sigma^2 \implies \alpha^p \propto \frac{\sigma^2}{\sum_{i \neq u} |\mathbf{h}_u^H \mathbf{w}_i^p|^2 P}. \quad (19)$$

Note that we need to compute an  $\alpha^p$  capable of balancing the interference terms across all users in such a way that the system's sum rate is maximized. Given this goal, we prioritize the user with the best channel conditions, i.e., the one that contributes the most to the sum rate. To this end, we select as reference the best performance indicator given by:

$$u^* = \arg \max_{u \in \mathcal{U}} \frac{|\mathbf{h}_u^H \mathbf{w}_u^p|^2 P}{\sum_{i \neq u} |\mathbf{h}_u^H \mathbf{w}_i^p|^2 P + \sigma^2}. \quad (20)$$

After determining the reference user, we perform the private power allocation as  $\alpha^p = \frac{\eta \sigma^2}{\sum_{i \neq u^*} |\mathbf{h}_{u^*}^H \mathbf{w}_i^p|^2 P}$ . The common power coefficient is consequently given by:

$$\alpha^c = 1 - U \alpha^p = 1 - \frac{U \eta \sigma^2}{\sum_{i \neq u^*} |\mathbf{h}_{u^*}^H \mathbf{w}_i^p|^2 P}, \quad (21)$$

where the scaling factor  $\eta$  adjusts the aggressiveness of the allocation, i.e., a higher  $\eta$  increases private power allocation, while a lower  $\eta$  reserves more power for the common message.

Thus, the original formulation can be transformed into a simpler version with a single optimization variable,  $\eta$ , resulting in the following relaxed power allocation problem:

$$\max_{\eta} R^c(\eta) + \sum_{u \in \mathcal{U}} R_u^p(\eta), \quad (22a)$$

$$\text{s.t. } \alpha^p = \frac{\eta \sigma^2}{\sum_{i \neq u^*} |\mathbf{h}_{u^*}^H \mathbf{w}_i^p|^2 P}, \quad (22b)$$

$$\alpha^c = 1 - U \alpha^p, \quad (22c)$$

$$U \alpha^p \geq 0, \quad \alpha^c \geq 0, \quad (22d)$$

where  $R^c(\eta)$  and  $R_u^p(\eta)$  denote the common and private rates as functions of  $\eta$ . Although the problem remains non-convex due to the minimum operator in the common rate and the nonlinear dependence of the SINRs on  $\eta$ , a linear search over  $\eta$  within its feasible range provides a practical and efficient method to approximate the solution of (22). Specifically, if  $\eta$  is chosen such that  $0 \leq \eta \leq \frac{\sum_{i \neq u^*} |\mathbf{h}_{u^*}^H \mathbf{w}_i^p|^2 P}{U \sigma^2}$ , the constraints in (22d) are automatically satisfied.

#### IV. DESIGN OF BD-RIS-INDUCED ATTACKS

The malicious goal of the attacker is to compute a reflection matrix  $\Theta$  that degrades the performance of the employed RSMA scheme. In the following subsections, we investigate two approaches to accomplish the goal.

##### A. Random interference attack

A simple yet effective method to degrade the performance of RSMA involves randomly configuring the reflection coefficients of an adversarial RIS to introduce interference, as demonstrated in our previous work with diagonal RISs [6].

a) *Fully connected architecture*: As explained, a fully connected RIS requires its reflection matrix to be both symmetric and unitary. To obtain a valid set of reflection coefficients, the adversary starts by creating a random complex matrix  $\tilde{\Gamma} \in \mathbb{C}^{D \times D}$  and then symmetrizes it, as follows:

$$\Gamma = \frac{1}{2} (\tilde{\Gamma} + \tilde{\Gamma}^T). \quad (23)$$

However,  $\Gamma$  is generally not unitary. Therefore, we need to project it onto the set of symmetric unitary matrices while respecting its symmetry constraint. To this end, we can rely on the Takagi factorization, which is introduced next.

*Property I*: Let  $\Gamma$  be a symmetric complex matrix. Then, the Takagi factorization states that there exists a unitary matrix  $\mathbf{U}_\Gamma$  and a diagonal matrix  $\Sigma_\Gamma$  such that  $\Gamma = \mathbf{U}_\Gamma \Sigma_\Gamma \mathbf{U}_\Gamma^T$ , where the diagonal entries of  $\Sigma_\Gamma$  are nonnegative singular values of  $\Gamma$ , called Takagi values, and the columns of  $\mathbf{U}_\Gamma$  are the associated orthonormal Takagi vectors. With Property I, the desired symmetric unitary reflection matrix can be achieved through the following lemma.

*Lemma I*: Let  $\Gamma$  be a complex symmetric matrix that admits the Takagi factorization  $\Gamma = \mathbf{U}_\Gamma \Sigma_\Gamma \mathbf{U}_\Gamma^T$ . Then, the unique symmetric unitary matrix

$$\Theta = \mathbf{U}_\Gamma \mathbf{U}_\Gamma^T, \quad (24)$$

minimizes the Frobenius norm  $\|\Gamma - \Theta\|_F$  and, thus, defines the optimal projection onto the set of symmetric unitary matrices.

*Proof*: Since  $\Gamma$  is complex symmetric, its Takagi factorization is given by  $\Gamma = \mathbf{U}_\Gamma \Sigma_\Gamma \mathbf{U}_\Gamma^T$ . Any symmetric unitary matrix can be written in the form  $\Theta = \mathbf{U}_\Gamma \mathbf{D} \mathbf{U}_\Gamma^T$ , where  $\mathbf{D}$  is a diagonal matrix with entries on the unit circle, i.e.,  $|\mathbf{D}_{ii}| = 1$ , for each diagonal element. The problem of finding the symmetric unitary matrix closest to  $\Gamma$  reduces to choosing  $\mathbf{D}$  such that

$$\begin{aligned} \|\Gamma - \Theta\|_F &= \|\mathbf{U}_\Gamma \Sigma_\Gamma \mathbf{U}_\Gamma^T - \mathbf{U}_\Gamma \mathbf{D} \mathbf{U}_\Gamma^T\|_F \\ &= \|\Sigma_\Gamma - \mathbf{D}\|_F \end{aligned} \quad (25)$$

is minimized, where the last equality follows from the unitary invariance of the Frobenius norm. Since each diagonal entry  $[\Sigma_\Gamma]_{ii}$  is nonnegative, for each  $i$  the distance  $|\mathbf{D}_{ii} - [\Sigma_\Gamma]_{ii}|$  is minimized by choosing  $\mathbf{D}_{ii} = 1$ , as  $|\mathbf{D}_{ii} - e^{i\theta}|$  attains its minimum when  $\theta = 0$ . Therefore, the optimal projection is given by  $\mathbf{D} = \mathbf{I}$ , yielding  $\Theta = \mathbf{U}_\Gamma \mathbf{I} \mathbf{U}_\Gamma^T = \mathbf{U}_\Gamma \mathbf{U}_\Gamma^T$ , which, clearly, is symmetric since

$$\Theta^T = (\mathbf{U}_\Gamma \mathbf{U}_\Gamma^T)^T = \mathbf{U}_\Gamma \mathbf{U}_\Gamma^T = \Theta. \quad (26)$$

This completes the proof.  $\square$

The projection through the Takagi factorization respects both the symmetry and unitary constraints required by the fully connected RIS. For any invertible complex symmetric matrix with distinct singular values, the Takagi factorization can be implemented very efficiently by aligning the phases of the singular vectors computed via the SVD [28].

*b) Group-connected architecture:* A similar strategy can be extended for a group-connected RIS architecture. In this case, the attacker must respect the group-wise constraints. Specifically, the reflection matrix  $\Theta$  should be block-diagonal, comprising  $G$  independent sub-matrices  $\Theta_g$ , for  $g = 1, \dots, G$ , each one being symmetric and unitary. To generate such a matrix, the adversary follows the same process as for the fully connected RIS, but now for each group. First, it constructs random complex matrices  $\tilde{\Gamma}_g \in \mathbb{C}^{D_g \times D_g}$  for every group. Then, symmetrized versions  $\Gamma_g$  are achieved as in (23). Subsequently, the Takagi factorization is computed for each symmetrized matrix, as  $\Gamma_g = \mathbf{U}_{\Gamma_g} \Sigma_{\Gamma_g} \mathbf{U}_{\Gamma_g}^T$ . The symmetric unitary matrix for the  $g$ th group is then obtained via the projection  $\Theta_g = \mathbf{U}_{\Gamma_g} \mathbf{U}_{\Gamma_g}^T$ , as in Lemma I. Finally, the full reflection matrix is assembled by organizing the  $G$  sub-matrices into a block-diagonal structure, i.e.,  $\Theta = \text{bdiag}(\Theta_1, \dots, \Theta_G)$ .

### B. Aligned interference attack

A more sophisticated adversarial strategy is to optimize the BD-RIS reflection coefficients to maximize the interference induced at the users. As demonstrated in [6] for conventional RIS systems, if the adversary can acquire partial RIS-associated CSI, it becomes possible to strategically steer the reflected power toward the users. In this subsection, we generalize such optimized attacks to BD-RIS architectures.

*a) Fully connected architecture:* Let  $\mu_i \in (0, 1]$  denote the adversarial weight assigned to user  $i \in \mathcal{U}$ . The malicious fully connected RIS controller aims to maximize the weighted sum of interference powers received at users, subject to unitary and symmetry constraints. Formally, the optimization problem can be formulated as:

$$\max_{\Theta} \sum_{i \in \mathcal{U}} \mu_i \|\mathbf{g}_i^H \Theta \mathbf{G}\|_2^2, \quad (27a)$$

$$\text{s.t. } \Theta = \Theta^T. \quad (27b)$$

$$\Theta^H \Theta = \mathbf{I}, \quad (27c)$$

The unitary constraint in (27c) defines a non-convex Stiefel manifold. This, combined with the quadratic dependence of the objective function on  $\Theta$ , makes the problem challenging to solve optimally. To simplify the original problem, we start by addressing the symmetry constraint in (27b). To this end, we exploit the mathematical structure of symmetric matrices by vectorizing  $\Theta$  using the concept of duplication matrix.

*Property II:* For any symmetric matrix  $\Theta$ , there exists a duplication matrix  $\mathbf{D} \in \mathbb{R}^{D^2 \times \frac{D(D+1)}{2}}$  that maps the half-vectorization of  $\Theta$  to its full vectorization:

$$\text{vec}(\Theta) = \mathbf{D} \text{vech}(\Theta), \quad (28)$$

#### Algorithm 1: Aligned Interference Attack for Fully Connected RIS

**Input:** Channel matrix  $\mathbf{G}$ , user channels  $\{\mathbf{g}_i\}_{i \in \mathcal{U}}$ , duplication matrix  $\mathbf{D}$ , user weights  $\{\mu_i\}_{i \in \mathcal{U}}$

**Output:** Optimized reflection matrix  $\Theta^*$

- 1 Compute the transformed interference channel matrices:
- 2 **foreach**  $i \in \mathcal{U}$  **do**
- 3   Compute:  $\mathbf{S}_i \leftarrow (\mathbf{G}^T \otimes \mathbf{g}_i^H)$ ;
- 4 Construct the weighted interference matrix:
 
$$\mathbf{S} \leftarrow [\sqrt{\mu_1} \mathbf{S}_1^H, \dots, \sqrt{\mu_U} \mathbf{S}_U^H]^H.$$
- 5 Compute the SVD of  $\tilde{\mathbf{S}} = \mathbf{S} \mathbf{D}$  to solve the relaxed problem in (32):
 
$$\tilde{\mathbf{S}} = \mathbf{U}_{\tilde{\mathbf{S}}} \Sigma_{\tilde{\mathbf{S}}} \mathbf{V}_{\tilde{\mathbf{S}}}^H.$$
- 6 Obtain the optimized reduced coefficient vector:  $\boldsymbol{\theta} \leftarrow \mathbf{v}_{\tilde{\mathbf{S}}, 1}$ , where  $\mathbf{v}_{\tilde{\mathbf{S}}, 1}$  is the corresponding dominant right singular vector.
- 7 Construct the relaxed reflection matrix:  $\Phi \leftarrow \text{unvec}(\mathbf{D} \boldsymbol{\theta})$ .
- 8 Perform the Takagi factorization:  $\Phi = \mathbf{U}_{\Phi} \Sigma_{\Phi} \mathbf{U}_{\Phi}^T$ .
- 9 Project onto the set of unitary matrices:  $\Theta^* \leftarrow \mathbf{U}_{\Phi} \mathbf{U}_{\Phi}^T$ .
- 10 **return**  $\Theta^*$ .

where the duplication matrix  $\mathbf{D}$  is uniquely defined as a sparse matrix with binary entries, given by:

$$\mathbf{D}^T \triangleq \sum_{i=1}^D \sum_{j=1}^i \mathbf{u}_{ij} \text{vec}(\mathbf{T}_{ij})^T, \quad (29)$$

where  $\mathbf{u}_{ij}$  is a unit vector of length  $\frac{D(D+1)}{2}$  with a single non-zero entry at position  $[(j-1)D + i - \frac{j(j-1)}{2}]$ , and  $\mathbf{T}_{ij}$  is a  $D \times D$  matrix with ones at positions  $(i, j)$  and  $(j, i)$ , and zeros elsewhere [29, Definitions 3.2a and 3.2b].

Property II inherently satisfies the symmetry constraint of the original formulation, allowing us to reformulate the problem in a simpler relaxed version in terms of  $\text{vech}(\Theta)$ .

Using the Kronecker product identity  $\text{vec}(\mathbf{A} \Theta \mathbf{C}) = (\mathbf{C}^T \otimes \mathbf{A}) \text{vec}(\Theta)$ , and invoking the duplication matrix relation in (28), we can vectorize the interference channels  $\mathbf{g}_i^H \Theta \mathbf{G}$  as:

$$\text{vec}(\mathbf{g}_i^H \Theta \mathbf{G}) = (\mathbf{G}^T \otimes \mathbf{g}_i^H) \mathbf{D} \text{vech}(\Theta). \quad (30)$$

Then, by defining  $\mathbf{S}_i = (\mathbf{G}^T \otimes \mathbf{g}_i^H) \in \mathbb{C}^{M \times D^2}$ , and letting  $\boldsymbol{\theta} = \text{vech}(\Theta) \in \mathbb{C}^{\frac{D(D+1)}{2}}$  denote the reduced vector of unique reflection coefficients, the objective function in (27a) becomes:

$$\begin{aligned} & \sum_{i \in \mathcal{U}} \mu_i \|(\mathbf{G}^T \otimes \mathbf{g}_i^H) \mathbf{D} \boldsymbol{\theta}\|_2^2 \\ &= \sum_{i \in \mathcal{U}} \mu_i \|\mathbf{S}_i \mathbf{D} \boldsymbol{\theta}\|_2^2 \\ &= \boldsymbol{\theta}^H \mathbf{D}^T \left( \sum_{i \in \mathcal{U}} \mu_i \mathbf{S}_i^H \mathbf{S}_i \right) \mathbf{D} \boldsymbol{\theta}. \end{aligned} \quad (31)$$

Given that  $\sum_{i \in \mathcal{U}} \mathbf{S}_i^H \mathbf{S}_i = [\mathbf{S}_1^H, \dots, \mathbf{S}_U^H]^H [\mathbf{S}_1^H, \dots, \mathbf{S}_U^H]$ , we can define the tall weighted interference matrix:  $\mathbf{S} \triangleq [\sqrt{\mu_1} \mathbf{S}_1^H, \dots, \sqrt{\mu_U} \mathbf{S}_U^H]^H \in \mathbb{C}^{U \times D^2}$  and rewrite the expression in (31) as the convex quadratic objective  $\boldsymbol{\theta}^H \mathbf{D}^T \mathbf{S}^H \mathbf{S} \mathbf{D} \boldsymbol{\theta}$ . This vectorized reformulation automatically satisfies the symmetry constraint in (27b) by construction. On the other hand, the non-convex unitary constraint in (27c) is relaxed with a

**Algorithm 2:** Aligned Interference Attack for Group-Connected RIS

**Input:** Channel matrix  $\mathbf{G}$ , user channels  $\{\mathbf{g}_i\}_{i \in \mathcal{U}}$ , RIS group indices  $\{\mathcal{E}_g\}_{g \in \mathcal{G}}$ , duplication matrices  $\{\mathbf{D}_g\}_{g \in \mathcal{G}}$ , user weights  $\{\mu_i\}_{i \in \mathcal{U}}$   
**Output:** Optimized block-diagonal reflection matrix  $\Theta^*$

- 1 Preprocess each RIS group:
- 2 **foreach**  $g \in \mathcal{G}$  **do**
- 3      $D_g \leftarrow |\mathcal{E}_g|$ ;
- 4     Extract BS-RIS subchannel:  $\mathbf{G}_g \leftarrow [\mathbf{G}]_{\mathcal{E}_g, :}$ ;
- 5     **foreach**  $i \in \mathcal{U}$  **do**
- 6         Extract RIS-user subchannel:  $\mathbf{g}_{ig} \leftarrow [\mathbf{g}_i]_{\mathcal{E}_g}$ ;
- 7         Compute:  $\mathbf{S}_{ig} \leftarrow (\mathbf{G}_g^T \otimes \mathbf{g}_{ig}^H)$ ;
- 8 Construct the interference matrix from group contributions:
- 9 **foreach**  $i \in \mathcal{U}$  **do**
- 10     Compute the block-row matrix:
 
$$\mathbf{J}_i \leftarrow [\mathbf{S}_{i1}\mathbf{D}_1 \quad \mathbf{S}_{i2}\mathbf{D}_2 \quad \cdots \quad \mathbf{S}_{iG}\mathbf{D}_G].$$
- 11 Construct the stacked global matrix:
 
$$\mathbf{J} \leftarrow [\sqrt{\mu_1}\mathbf{J}_1^T, \sqrt{\mu_2}\mathbf{J}_2^T, \cdots, \sqrt{\mu_U}\mathbf{J}_U^T]^T.$$
- 12 Compute the SVD of  $\mathbf{J}$  to solve the relaxed problem in (43):
 
$$\mathbf{J} = \mathbf{U}_J \Sigma_J \mathbf{V}_J^H.$$
- 13 Obtain the optimized coefficient vector:  $\varphi \leftarrow \mathbf{v}_{\mathbf{J},1}$ , where  $\mathbf{v}_{\mathbf{J},1}$  is the corresponding dominant right singular vector.
- 14 **foreach**  $g \in \mathcal{G}$  **do**
- 15     Extract reduced vector:  $\theta_g \leftarrow [\varphi]_{\mathcal{R}_g}$ , where  $\mathcal{R}_g \subset \{1, \dots, \sum_{g \in \mathcal{G}} \frac{D_g(D_g+1)}{2}\}$  is the index set for group  $g$ , with  $|\mathcal{R}_g| = \frac{D_g(D_g+1)}{2}$ .
- 16     Construct the relaxed reflection matrix:  $\Phi_g \leftarrow \text{unvec}(\mathbf{D}_g \theta_g)$ .
- 17     Perform the Takagi factorization:  $\Phi_g = \mathbf{U}_{\Phi_g} \Sigma_{\Phi_g} \mathbf{U}_{\Phi_g}^T$ .
- 18     Project onto the set of unitary matrices:  $\Theta_g^* \leftarrow \mathbf{U}_{\Phi_g} \mathbf{U}_{\Phi_g}^T$ .
- 19 Construct the final block-diagonal reflection matrix:
 
$$\Theta^* \leftarrow \text{bdiag}(\Theta_1^*, \Theta_2^*, \dots, \Theta_G^*).$$
- 20 **return**  $\Theta^*$ .

convex  $\ell_2$ -norm bound  $\|\theta\|_2 \leq 1$ , which allow us to formulate a tractable optimization problem:

$$\max_{\theta} \theta^H \mathbf{D}^T \mathbf{S}^H \mathbf{S} \mathbf{D} \theta \quad (32a)$$

$$\text{s.t. } \|\theta\|_2 \leq 1. \quad (32b)$$

This relaxed problem (32) constitutes a QCQP, whose optimal solution is the dominant right singular vector of the matrix  $\tilde{\mathbf{S}} \triangleq \mathbf{S} \mathbf{D}$ . More specifically, by recalling the SVD, we can express  $\tilde{\mathbf{S}} = \mathbf{U}_{\tilde{\mathbf{S}}} \Sigma_{\tilde{\mathbf{S}}} \mathbf{V}_{\tilde{\mathbf{S}}}^H$ , where  $\mathbf{V}_{\tilde{\mathbf{S}}} = [\mathbf{v}_{\tilde{\mathbf{S}},1}, \mathbf{v}_{\tilde{\mathbf{S}},2}, \dots, \mathbf{v}_{\tilde{\mathbf{S}}, \frac{D(D+1)}{2}}]$  contains the right singular vectors. Then, the optimal solution to the relaxed problem is given by  $\theta = \mathbf{v}_{\tilde{\mathbf{S}},1}$ , thus satisfying  $\|\theta\|_2 = 1$ , and the corresponding relaxed BD-RIS matrix is obtained by:

$$\Phi = \text{unvec}(\mathbf{D}\theta). \quad (33)$$

However,  $\Phi$  generally violates the unitary constraint, i.e.,  $\Phi^H \Phi \neq \mathbf{I}$ . To enforce this, we project  $\Phi$  onto the closest unitary matrix via the Takagi factorization explained in Property I, i.e.,  $\Phi = \mathbf{U}_{\Phi} \Sigma_{\Phi} \mathbf{U}_{\Phi}^T$ , allowing us to compute

$$\Theta^* = \mathbf{U}_{\Phi} \mathbf{U}_{\Phi}^T, \quad (34)$$

where, according to Lemma I, the symmetry is preserved.

b) *Group-connected architecture:* The aligned interference attack is now generalized for the group-connected architecture. Let us consider a BD-RIS partitioned into  $G$  independent groups, i.e.,  $\Theta = \text{bdiag}(\Theta_1, \dots, \Theta_G)$ , with each block satisfying  $\Theta_g = \Theta_g^T$  and  $\Theta_g^H \Theta_g = \mathbf{I}$ . Then, the optimized adversary attack strategy can be formulated as:

$$\max_{\Theta} \sum_{i \in \mathcal{U}} \mu_i \|\mathbf{g}_i^H \Theta \mathbf{G}\|_2^2, \quad (35a)$$

$$\text{s.t. } \Theta = \text{bdiag}(\Theta_1, \dots, \Theta_G), \quad (35b)$$

$$\Theta_g = \Theta_g^T, \quad (35c)$$

$$\Theta_g^H \Theta_g = \mathbf{I}. \quad (35d)$$

To address problem 35, the first step is to decompose the global channel matrices into group-specific subchannels. To this end, let  $\mathcal{E}_g \subset \{1, \dots, D\}$  denote the index subset of RIS elements associated with group  $g$ , with  $|\mathcal{E}_g| = D_g$ . Then, the BS-RIS subchannel for group  $g$  can be expressed as

$$\mathbf{G}_g = [\mathbf{G}]_{\mathcal{E}_g, :} \in \mathbb{C}^{D_g \times M}, \quad (36)$$

while the RIS-user subchannel becomes

$$\mathbf{g}_{ig} = [\mathbf{g}_i]_{\mathcal{E}_g} \in \mathbb{C}^{D_g}. \quad (37)$$

Next, following Property II, we construct a duplication matrix  $\mathbf{D}_g \in \mathbb{R}^{D_g \times \frac{D_g(D_g+1)}{2}}$  to vectorize the symmetric matrix as  $\text{vec}(\Theta_g) = \mathbf{D}_g \theta_g$  for each group, where  $\theta_g = \text{vech}(\Theta_g) \in \mathbb{C}^{\frac{D_g(D_g+1)}{2}}$  denotes the  $g$ th reduced coefficient vector. We also define  $\mathbf{S}_{ig} = (\mathbf{G}_g^T \otimes \mathbf{g}_{ig}^H) \in \mathbb{C}^{M \times D_g}$ , and represent the set of RIS groups by  $\mathcal{G} = \{1, \dots, G\}$ . Then, we rewrite the adversary objective as follows:

$$\begin{aligned} \sum_{i \in \mathcal{U}} \mu_i \left\| \sum_{j \in \mathcal{G}} (\mathbf{G}_j^T \otimes \mathbf{g}_{ij}^H) \mathbf{D}_j \theta_j \right\|_2^2 \\ = \sum_{i \in \mathcal{U}} \mu_i \left\| \sum_{j \in \mathcal{G}} \mathbf{S}_{ij} \mathbf{D}_j \theta_j \right\|_2^2. \end{aligned} \quad (38)$$

To further simplify, we introduce a global stacked vector:

$$\varphi \triangleq [\theta_1^T, \theta_2^T, \dots, \theta_G^T]^T \in \mathbb{C}^{\sum_{g \in \mathcal{G}} \frac{D_g(D_g+1)}{2}}, \quad (39)$$

and define, for each user  $i \in \mathcal{U}$ , the block row matrix:

$$\mathbf{J}_i \triangleq [\mathbf{S}_{i1}\mathbf{D}_1, \mathbf{S}_{i2}\mathbf{D}_2, \dots, \mathbf{S}_{iG}\mathbf{D}_G]. \quad (40)$$

Now, the summation related to the groups can be written as a single matrix structure, as follows:

$$\begin{aligned} \sum_{i \in \mathcal{U}} \mu_i \left\| \sum_{j \in \mathcal{G}} \mathbf{S}_{ij} \mathbf{D}_j \theta_j \right\|_2^2 \\ = \varphi^H \left( \sum_{i \in \mathcal{U}} \mu_i \mathbf{J}_i^H \mathbf{J}_i \right) \varphi. \end{aligned} \quad (41)$$

Then, we define a global matrix  $\mathbf{J}$  stacking all  $\mathbf{J}_i$  matrices:

$$\mathbf{J} \triangleq [\sqrt{\mu_1}\mathbf{J}_1^T, \sqrt{\mu_2}\mathbf{J}_2^T, \dots, \sqrt{\mu_U}\mathbf{J}_U^T]^T. \quad (42)$$

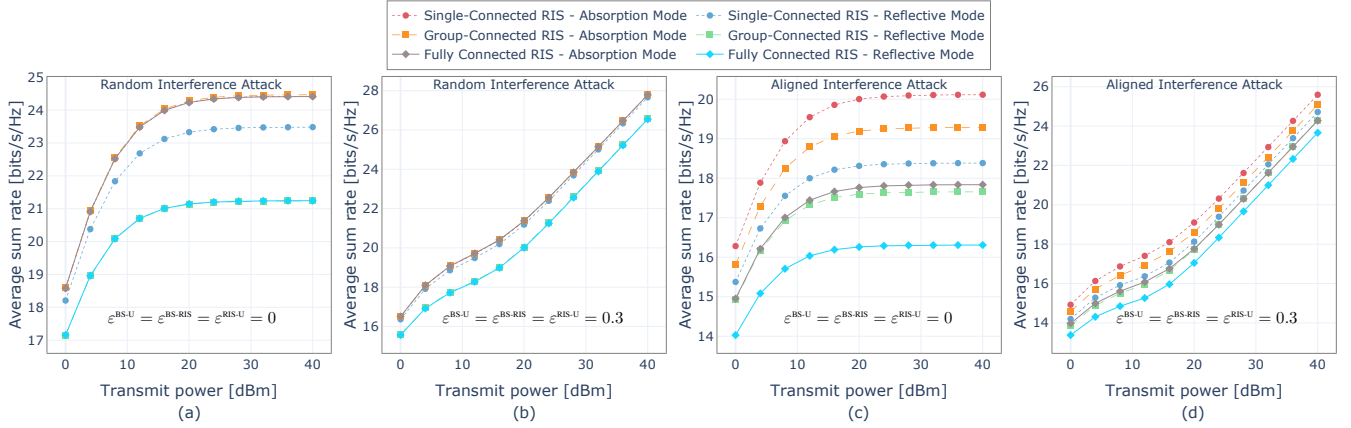


Fig. 3: Impact of the RIS operation mode during the uplink training phase on the RSMA average sum rate, with  $D = 200$  reflecting elements. Subfigures (a) and (b) illustrate the case of *Random Interference Attacks*, while (c) and (d) correspond to *Aligned Interference Attacks*. Perfect CSI is assumed in all links for subfigures (a) and (c), whereas subfigures (b) and (d) consider imperfect CSI, with the channel errors set to  $\varepsilon^{\text{BS-U}} = \varepsilon^{\text{BS-RIS}} = \varepsilon^{\text{RIS-U}} = 0.3$ .

This allows us to write the summation in (41) in its matrix-equivalent form, resulting in the final compact problem:

$$\max_{\varphi} \quad \varphi^H \mathbf{J}^H \mathbf{J} \varphi, \quad (43a)$$

$$\text{s.t.} \quad \|\varphi\|_2 \leq 1. \quad (43b)$$

The solution to (43) can be obtained with the aid of the SVD, similarly to the problem (32). More specifically, we can decompose  $\mathbf{J} = \mathbf{U}_J \Sigma_J \mathbf{V}_J^H$  and achieve the desired solution by computing  $\varphi = \mathbf{v}_{J,1}$ , where  $\mathbf{v}_{J,1}$  is the dominant right singular vector of  $\mathbf{J}$ , i.e., the first column of  $\mathbf{V}_J$ . Finally, by letting  $\mathcal{R}_g \subset \left\{ 1, \dots, \sum_{g \in \mathcal{G}} \frac{D_g(D_g+1)}{2} \right\}$  denote the index subset corresponding to the  $g$ th reduced coefficient vector, with  $|\mathcal{R}_g| = \frac{D_g(D_g+1)}{2}$ , the relaxed coefficients for each independent RIS group can be obtained as  $\theta_g = [\varphi]_{\mathcal{R}_g}$ , and  $\Phi_g = \text{unvec}(\mathbf{D}_g \theta_g)$ ,  $\forall g \in \mathcal{G}$ . Recalling Property I, we compute the Takagi factorization  $\Phi_g = \mathbf{U}_{\Phi_g} \Sigma_{\Phi_g} \mathbf{U}_{\Phi_g}^T$  and project each  $\Phi_g$  onto its closest unitary matrix, as follows:

$$\Theta_g^* = \mathbf{U}_{\Phi_g} \mathbf{U}_{\Phi_g}^T. \quad (44)$$

Finally, the full BD-RIS reflection matrix is constructed as  $\Theta^* = \text{bdiag}(\Theta_1^*, \dots, \Theta_G^*)$ .

## V. NUMERICAL RESULTS

In this section, we evaluate the impact of BD-RIS-induced attacks under both random and optimized strategies and investigate RSMA's ability to maintain performance under adversarial conditions. We investigate the degradations induced by fully connected, group-connected, and conventional single-connect RIS architectures and provide a comprehensive performance comparison with SDMA.

The simulation setup comprises: (i) a BS equipped with  $M = 32$  transmit antennas positioned at the origin, (ii) three users located at distances of  $d_1 = 30$  m,  $d_2 = 50$  m, and  $d_3 = 60$  m from the BS, with corresponding azimuth angles of  $\theta_1 = 25^\circ$ ,  $\theta_2 = 15^\circ$ , and  $\theta_3 = 10^\circ$ , and (iii) the adversarial RIS deployed a distance  $d_{\text{RIS}} = 40$  m apart from the BS with

an azimuth angle of  $\theta_{\text{RIS}} = 5^\circ$ . Simulations are performed for various numbers of reflecting elements, with the group-connected RIS architecture configured as  $D_1 = \dots = D_G = 5$ . All links follow a power-law path loss model  $d^{-\eta}$  with  $\eta = 3$ , where  $d$  represents the corresponding distance. In particular, the distance from the RIS to the  $u$ th user can be obtained by  $d_{\text{RIS},u} = \sqrt{d_{\text{RIS}}^2 + d_u^2 - 2d_{\text{RIS}}d_u \cos(\theta_{\text{RIS}} - \theta_u)}$ , resulting in the distances  $d_{\text{RIS},1} \approx 15.64$  m,  $d_{\text{RIS},2} \approx 12.68$  m, and  $d_{\text{RIS},3} \approx 20.45$  m. Moreover, the user weights for Algorithms 1 and 2 are set uniformly as  $\mu_1 = \mu_2 = \mu_3 = 1/3$ , the noise variance is set to  $\sigma^2 = -60$  dB, and the SDMA scheme employs uniform power allocation with regularized zero-forcing precoders.

Fig. 3 investigates the impact of the RIS operation mode during the training phase on the RSMA average sum rate for different RIS architectures with  $D = 200$  reflecting elements, under both perfect and imperfect CSI. It can be seen in all subfigures that using reflective mode during uplink training leads to lower average sum rates. This applies to both perfect CSI, Figs. 3(a) and 3(c), and imperfect CSI cases, Figs. 3(b) and 3(d). This training mode choice significantly boosts the degradation potential for all RIS architectures, but the benefit for the attacker is largest when using BD-RISs. Even under random interference attacks, group-connected and fully connected architectures cause significantly more degradation than a single-connected RIS if the reflective mode training is employed, which can be observed in both Figs. 3(a) and 3(b). The degradations under aligned interference attacks in Fig. 3(c) are even greater, with the fully connected RIS reducing the sum rate to approximately 16.3 bits/s/Hz at 40 dBm, which is significantly lower than the 18.4 bits/s/Hz achieved by the single-connected RIS employing the reflective training mode. This outcome suggests that operating the RIS in reflective mode during pilot transmission leads to more severe errors in the legitimate system's channel estimation. These errors, in turn, degrade the effectiveness of the private precoders and increase the impact of subsequent attacks, particularly for BD-RIS architectures due to their superior

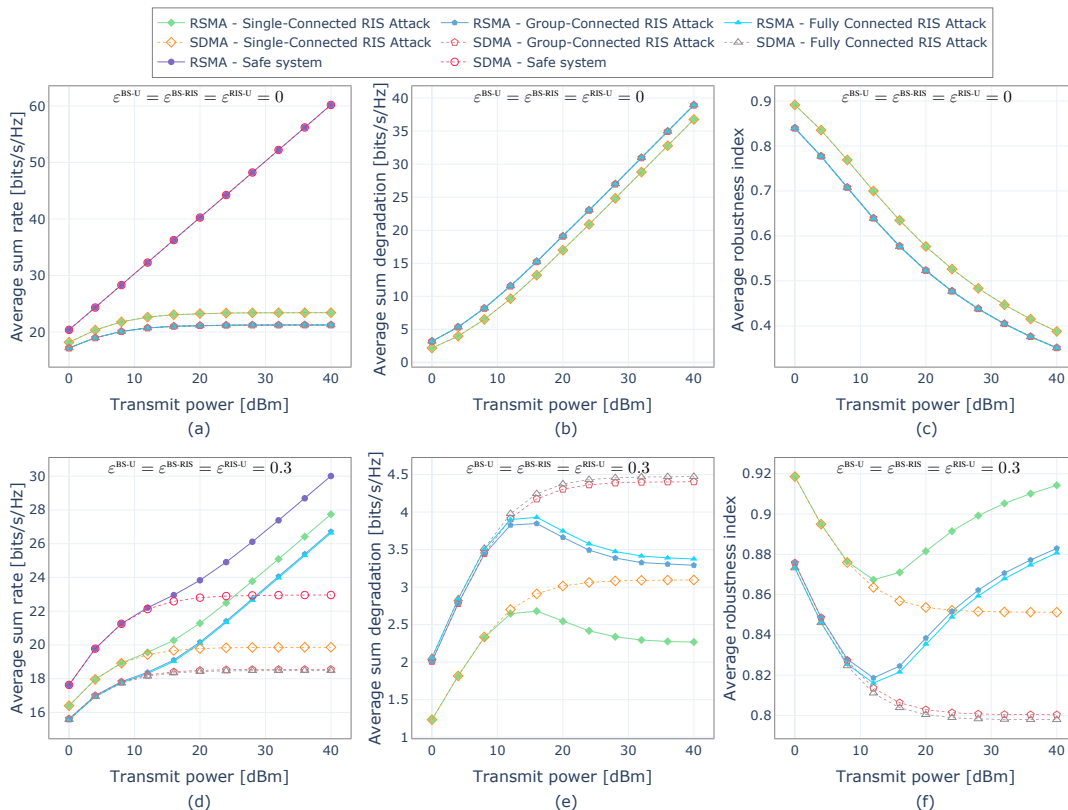


Fig. 4: System performance versus transmit power under *Random Interference Attacks* for different RIS architectures comprising  $D = 200$  reflecting elements. Results are presented in terms of: average sum rate in subfigures (a) and (d), average sum-rate degradation in (b) and (e), and average robustness index in (c) and (f). Subfigures (a)–(c) assume perfect CSI in all links, while subfigures (d)–(f) assume imperfect CSI with channel errors set to  $\epsilon^{\text{BS-U}} = \epsilon^{\text{BS-RIS}} = \epsilon^{\text{RIS-U}} = 0.3$ .

radiation efficiency. It is also worth noting that the results under imperfect CSI in Figs. 3(b) and 3(d) offer a glimpse into an important RSMA feature: its inherent robustness and potential for attack recovery thanks to the adaptive power allocation described in Section III-F.

Given that operating in reflective mode during uplink pilot training leads to more severe degradation, we adopt this mode in Fig. 4 and subsequent results. Fig. 4 compares the performance of RSMA and SDMA under random interference attacks versus varying transmit power levels. Figs. 4(a)–(c) depict the ideal scenario of perfect CSI at both the BS and the attacker. Fig. 4(a) shows that attacks via any RIS architecture force both RSMA and SDMA sum rate curves to saturate at high transmit powers, a behavior absent in the safe system baseline. Moreover, since RSMA reduces to SDMA under perfect CSI conditions, the two schemes exhibit identical performance under both safe and attack scenarios, corroborating intuition and previously reported results [9]. Fig. 4(a) also reinforces why an attacker might choose a BD-RIS: group-connected and fully-connected architectures induce larger performance degradations (saturating near 21 bits/s/Hz) than single-connected RISs (saturating near 23 bits/s/Hz). This trend also manifests in Fig. 4(b), where the average sum-rate degradation, defined in (9), is consistently higher for BD-RIS attacks. In Fig. 4(c), the average robustness

index further confirms this behavior, with single-connected RIS attacks achieving approximately 0.39 at 40 dBm versus 0.35 for the BD-RISs at the same power level.

Shifting the focus to the imperfect CSI case in Figs. 4(d)–(f), the performance dynamics change considerably. Fig. 4(d) shows the average sum rate, highlighting two key aspects: first, RSMA now consistently achieves a significantly higher sum rate than SDMA under all attack scenarios, demonstrating its inherent robustness when channel knowledge is imperfect. Second, the performance difference due to the attacking RIS architecture becomes more pronounced. Attacks from the fully connected RIS yield the lowest sum rate, followed by the group-connected, with the single-connected RIS being the least detrimental. Fig. 4(e) shows the corresponding average sum-rate degradation and confirms that RSMA is less affected than SDMA across all RIS architectures, exhibiting significantly lower sum-rate degradation values. It is also reinforced that RSMA can partially recover from the attacks. The sum-rate degradation for RSMA peaks near 12 dBm and then decreases slightly as the transmit power gets higher – a trend not observed with SDMA. This behavior results in higher robustness index values for RSMA when transmit powers are greater than 12 dBm in Fig. 4(f). Furthermore, the robustness index is highest for single-connected and lowest for fully connected attacks.

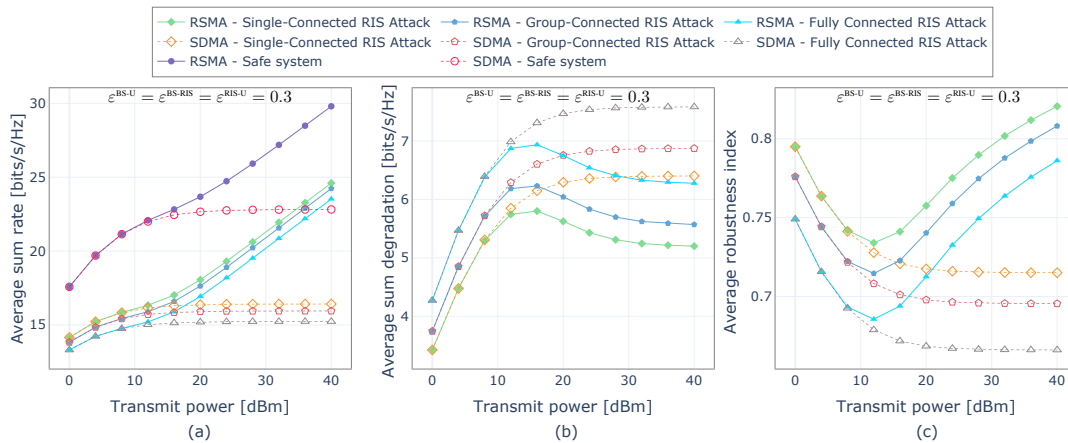


Fig. 5: System performance versus transmit power under *Aligned Interference Attacks* for different RIS architectures comprising  $D = 200$  reflecting elements. Results are presented in terms of: average sum rate in subfigure (a), average sum-rate degradation in (b), and average robustness index in (c). Results assume imperfect CSI with channel errors set to  $\epsilon^{\text{BS-U}} = \epsilon^{\text{BS-RIS}} = \epsilon^{\text{RIS-U}} = 0.3$ .

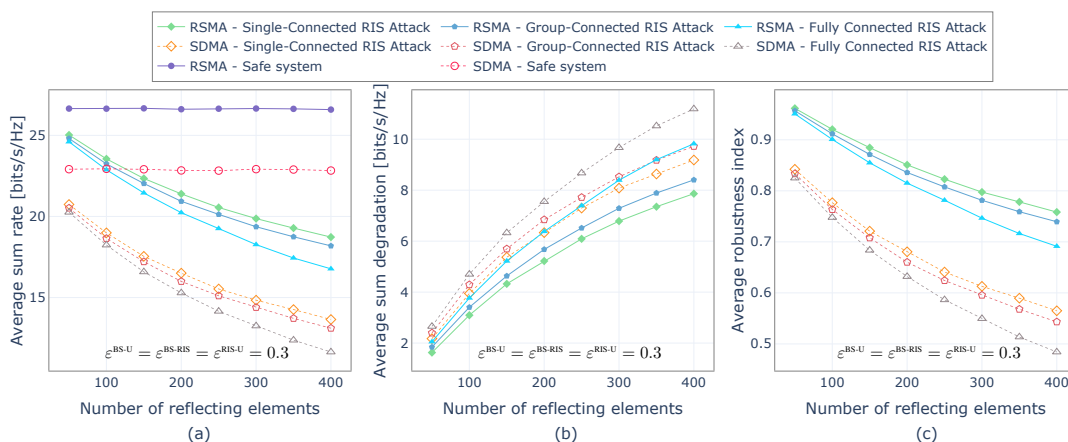


Fig. 6: System performance versus the number of reflecting elements under *Aligned Interference Attacks*, employing a transmit power of  $P = 30$  dBm and assuming imperfect CSI with channel errors set to  $\epsilon^{\text{BS-U}} = \epsilon^{\text{BS-RIS}} = \epsilon^{\text{RIS-U}} = 0.3$ . Results are presented in terms of: (a) average sum rate, (b) average sum-rate degradation, and (c) average robustness index.

Fig. 5 delves deeper into the impact of aligned interference attacks under imperfect CSI. As can be seen, the proposed optimized attack is highly effective, leading to more severe performance degradation on both RSMA and SDMA across the considered RIS architectures compared to the random interference in Fig. 4. For instance, RSMA under attack now struggles to exceed 24 bits/s/Hz even at high transmit power in Fig. 5(a), compared to nearly 28 bits/s/Hz under random attacks (Fig. 4(d)). SDMA, in particular, suffers drastically, with its sum-rate barely increasing with transmit power and remaining below 17 bits/s/Hz across all RIS architectures. Fig. 5(b) shows the average sum-rate degradation. Compared to random attacks (Fig. 4(e)), the degradation values are significantly higher for both schemes. RSMA still exhibits its characteristic robustness, with its degradation again peaking (now, around 15 dBm) before decreasing, indicating its mitigation capabilities even against these optimized attacks. In contrast, SDMA shows higher degradation levels that saturate at high transmit powers, highlighting its inability to recover

from the attacks. Consequently, in Fig. 5(c), RSMA achieves considerably higher robustness index values than SDMA, especially for transmit powers above 10 dBm.

Fig. 6 analyzes the impact of the adversarial RIS size  $D$  on system performance under aligned interference attacks, considering a fixed transmit power of 30 dBm and imperfect CSI. The detrimental effect of increasing the number of reflecting elements is markedly amplified under aligned attacks. As shown in Fig. 6(a), the sum rate of SDMA collapses at larger  $D$ , while the decline of RSMA is less severe. This is further evidenced in Fig. 6(b), where SDMA incurs substantially higher sum-rate degradation, and in Fig. 6(c), where the difference in robustness between RSMA and SDMA becomes particularly pronounced as  $D$  grows, highlighting RSMA's superior ability to cope with harmful interference. The relative impact of different RIS architectures follows the established trend, with BD-RISs inflicting the most damage. However, the aligned attack strategy enhances the effectiveness of all architectures, such that even attacks via single-connected RISs

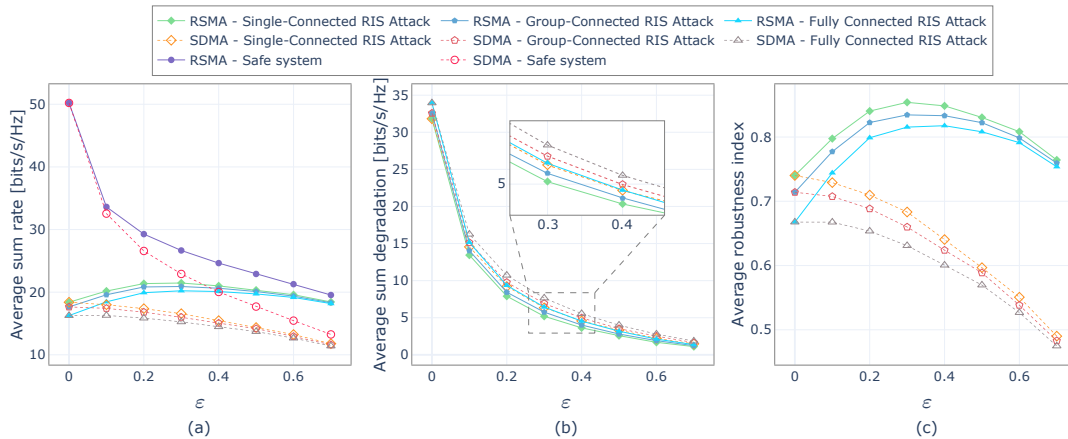


Fig. 7: System performance versus channel estimation error under *Aligned Interference Attacks*, employing a transmit power of  $P = 30$  dBm and assuming  $\varepsilon^{\text{BS-U}} = \varepsilon^{\text{BS-RIS}} = \varepsilon^{\text{RIS-U}} = \varepsilon$ . Results are presented in terms of: (a) average sum rate, (b) average sum-rate degradation, and (c) average robustness index.

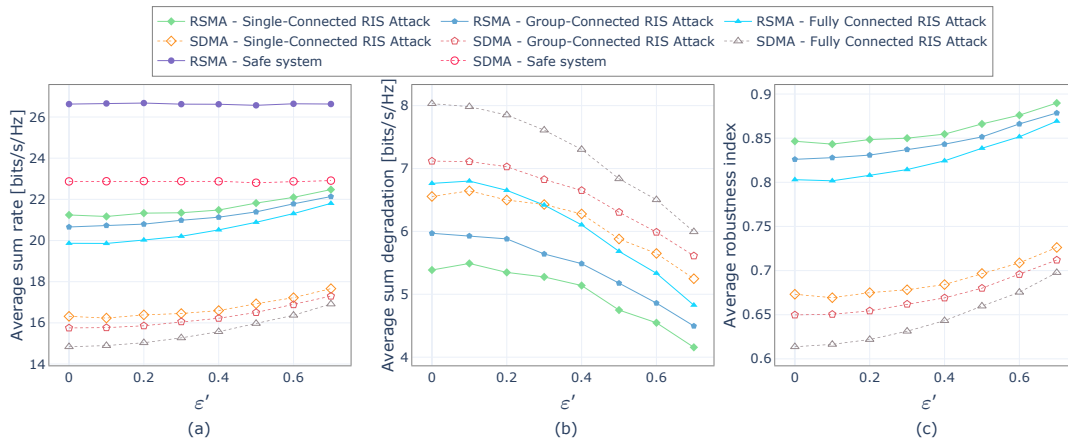


Fig. 8: System performance versus varying channel estimation errors under *Aligned Interference Attacks*, employing a transmit power of  $P = 30$  dBm and assuming  $\varepsilon^{\text{BS-RIS}} = \varepsilon^{\text{RIS-U}} = \varepsilon'$ , with a fixed error of  $\varepsilon^{\text{BS-U}} = 0.3$  in the BS-user link. Results are presented in terms of: (a) average sum rate, (b) average sum-rate degradation, and (c) average robustness index.

cause substantial performance loss, particularly for large  $D$ . We can also see that the performance curves for the different architectures are more distinctly separated across the range of  $D$ , confirming that the architectural choice of the attacking RIS is a significant factor, even more so under optimized attacks.

Fig. 7 presents the system response to aligned interference attacks versus varying channel estimation errors, assuming the error is uniform across all links, i.e.,  $\varepsilon^{\text{BS-U}} = \varepsilon^{\text{BS-RIS}} = \varepsilon^{\text{RIS-U}} = \varepsilon$ . As the channel estimation error  $\varepsilon$  increases, the safe system sum rate for both RSMA and SDMA decreases substantially. However, because of the smart power splitting of RSMA, it achieves superior performance throughout the error range. Under attack, Fig. 7(a) reveals that SDMA's sum rate monotonically decreases with increasing  $\varepsilon$ . On the other hand, RSMA's sum rate under attack exhibits a slight initial increase for small  $\varepsilon > 0$  before decreasing, suggesting its interference management adapts well to low to moderate channel error levels even under attack. The average sum-rate degradation in Fig. 7(b) shows a steep decrease as  $\varepsilon$  increases for all attacked scenarios. This is attributed to the drop in the

safe system's performance caused by imperfect CSI, which reduces the absolute difference between the safe and attacked performance levels. As for the average robustness index in Fig. 7(c), SDMA's curves under attack start at its highest value at  $\varepsilon = 0$  and decrease steadily as  $\varepsilon$  increases, dropping below 0.5 at high error levels. In contrast, RSMA displays a different trend, such that its robustness increases with lower values of  $\varepsilon$ , peaks around  $\varepsilon = 0.3$ , and then declines, although remaining significantly above SDMA's robustness for all  $\varepsilon > 0$ .

Fig. 8 isolates the effect of channel estimation errors specific to the RIS-related links ( $\varepsilon' = \varepsilon^{\text{BS-RIS}} = \varepsilon^{\text{RIS-U}}$ ) under aligned interference attacks, with the BS-User link error fixed at  $\varepsilon^{\text{BS-U}} = 0.3$ . As the error  $\varepsilon'$  increases, the performance of both SDMA and RSMA under attack improves. For instance, Figs. 8(a), (b), and (c) respectively show a slightly increasing average sum rate, a decreasing average sum-rate degradation, and an increasing average robustness index. This behavior comes from the fact that higher estimation errors ( $\varepsilon'$ ) lead to less accurate RIS configurations, resulting in less effectively aligned interference. Across all values of  $\varepsilon'$ , RSMA maintains

significantly higher sum rates and robustness, with lower degradation than SDMA. Furthermore, the relative impact of the RIS architectures persists despite the attacker's imperfect channel knowledge, with the fully connected RISs consistently delivering the strongest attacks.

## VI. CONCLUSIONS

This paper has investigated the robustness of RSMA-based multi-user MIMO systems to adversarial attacks induced by BD-RISs. Two effective attack strategies were described and studied: random and aligned interference. For each, novel algorithms were proposed to generate valid reflection coefficients respecting the architectural BD-RIS constraints. Extensive simulations revealed that RSMA demonstrated significantly greater robustness to these attacks than the benchmark SDMA scheme, especially under imperfect CSI. Moreover, BD-RIS significantly enhances adversarial efficacy compared to conventional RIS, with particularly severe performance degradation observed when the BD-RIS manipulates the uplink training phase via reflective operation. Future work should expand this analysis and investigate the adversarial potential of multi-sector BD-RISs and its non-reciprocal architectures. The development of robust countermeasures against such threats is another crucial direction.

## ACKNOWLEDGMENTS

This work was supported by the Commonwealth Cyber Initiative (cyberinitiative.org) in Virginia, US, an investment to advance cyber R&D, innovation, and workforce development, the National Science Foundation under grants no. 2326599 and 231879, and the Research Council of Finland through the 6G-ConCoRSe project (grant no. 359850) and the 6G Flagship programme (grant no. 369116).

## REFERENCES

- [1] B. Lyu, D. T. Hoang, S. Gong, D. Niyato, and D. I. Kim, "IRS-based wireless jamming attacks: When jammers can attack without power," *IEEE Wireless Commun. Lett.*, vol. 9, no. 10, pp. 1663–1667, 2020.
- [2] Y. Wang, H. Lu, D. Zhao, Y. Deng, and A. Nallanathan, "Wireless communication in the presence of illegal reconfigurable intelligent surface: Signal leakage and interference attack," *IEEE Wireless Commun. Mag.*, vol. 29, no. 3, pp. 131–138, 2022.
- [3] P. Staat, H. Elders-Boll, M. Heinrichs, C. Zenger, and C. Paar, "Mirror, mirror on the wall: Wireless environment reconfiguration attacks based on fast software-controlled surfaces," in *Proc. Asia Conf. on Computer and Communications Security*, 2022, pp. 208–221.
- [4] H. Alakoca, M. Namdar, S. Aldirmaz-Colak, M. Basaran, A. Basgumus, L. Durak-Ata, and H. Yanikomeroglu, "Metasurface Manipulation Attacks: Potential Security Threats of RIS-Aided 6G Communications," *IEEE Commun. Mag.*, vol. 61, no. 1, pp. 24–30, 2023.
- [5] H. Huang, Y. Zhang, H. Zhang, Y. Cai, A. L. Swindlehurst, and Z. Han, "Disco intelligent reflecting surfaces: Active channel aging for fully-passive jamming attacks," *IEEE Trans. Wireless Commun.*, vol. 23, no. 1, pp. 806–819, 2024.
- [6] A. S. de Sena, J. Kibilda, N. H. Mahmood, A. Gomes, and M. Latva-aho, "Malicious RIS versus massive MIMO: Securing multiple access against RIS-based jamming attacks," *IEEE Wireless Commun. Lett.*, vol. 13, no. 4, pp. 989–993, 2024.
- [7] H. Wang, Z. Han, and A. L. Swindlehurst, "Channel Reciprocity Attacks Using Intelligent Surfaces With Non-Diagonal Phase Shifts," *IEEE Open Journal of the Communications Society*, vol. 5, pp. 1469–1485, 2024.
- [8] S. Rivetti, O. T. Demir, E. Bjornson, and M. Skoglund, "Malicious Reconfigurable Intelligent Surfaces: How Impactful Can Destructive Beamforming be?" *IEEE Wireless Commun. Lett.*, vol. 13, no. 7, pp. 1918–1922, 2024.
- [9] A. S. de Sena, A. Gomes, J. Kibilda, N. H. Mahmood, L. A. DaSilva, and M. Latva-aho, "Malicious RIS Meets RSMA: Unveiling the Robustness of Rate Splitting to RIS-Induced Attacks," *IEEE Global Communications Conference (GlobeCom)*, pp. 3576–3581, 2024.
- [10] A. S. de Sena, P. H. J. Nardelli, D. B. da Costa, P. Popovski, and C. B. Papadias, "Rate-splitting multiple access and its interplay with intelligent reflecting surfaces," *IEEE Commun. Mag.*, vol. 60, no. 7, pp. 52–57, 2022.
- [11] B. Clerckx, Y. Mao, E. A. Jorswieck, J. Yuan, D. J. Love, E. Erkip, and D. Niyato, "A Primer on Rate-Splitting Multiple Access: Tutorial, Myths, and Frequently Asked Questions," *IEEE J. Sel. Areas Commun.*, vol. 41, no. 5, pp. 1265–1308, 2023.
- [12] H. Li, S. Shen, M. Nerini, and B. Clerckx, "Reconfigurable intelligent surfaces 2.0: Beyond diagonal phase shift matrices," *IEEE Commun. Mag.*, vol. 62, no. 3, pp. 102–108, 2023.
- [13] H. Huang, L. Dai, H. Zhang, C. Zhang, Z. Tian, Y. Cai, A. L. Swindlehurst, and Z. Han, "DISCO Might Not Be Funky: Random Intelligent Reflective Surface Configurations That Attack," *IEEE Wireless Commun. Mag.*, vol. 31, no. 5, pp. 76–82, 2024.
- [14] A. Gomes, A. S. de Sena, N. H. Mahmood, M. Latva-aho, L. A. DaSilva, and J. Kibilda, "Beam Management Manipulation with Adversarial Reconfigurable Intelligent Surfaces," in *IEEE GlobeCom*, 2024, pp. 3231–3236.
- [15] G. Li, P. Staat, H. Li, M. Heinrichs, C. Zenger, R. Kronberger, H. Elders-Boll, C. Paar, and A. Hu, "RIS-Jamming: Breaking Key Consistency in Channel Reciprocity-Based Key Generation," *IEEE Trans. Inf. Forensics Security*, vol. 19, pp. 5090–5105, 2024.
- [16] H. Wang, J. Nossek, and A. L. Swindlehurst, "Beyond-Diagonal RIS Attacks on Physical Layer Key Generation," in *IEEE International Workshop on Signal Processing Advances in Wireless Communications (SPAWC)*, 2024, pp. 946–950.
- [17] H. Huang, H. Zhang, W. Mei, J. Li, Y. Cai, A. L. Swindlehurst, and Z. Han, "Integrated Sensing and Communication Under DISCO Physical-Layer Jamming Attacks," *IEEE Wireless Commun. Lett.*, vol. 13, no. 11, pp. 3044–3048, 2024.
- [18] S. Rivetti, O. T. Demir, E. Bjornson, and M. Skoglund, "Destructive and constructive RIS beamforming in an ISAC-multi-user MIMO network," *arXiv preprint arXiv:2404.11314*, 2024.
- [19] G. Zhou, Y. Mao, and B. Clerckx, "Rate-splitting multiple access for multi-antenna downlink communication systems: Spectral and energy efficiency tradeoff," *IEEE Trans. Wireless Commun.*, vol. 21, no. 7, pp. 4816–4828, 2022.
- [20] H. Lu, X. Xie, Z. Shi, H. Lei, N. Zhao, and J. Cai, "Outage Performance of Uplink Rate Splitting Multiple Access With Randomly Deployed Users," *IEEE Trans. Wireless Commun.*, vol. 23, no. 2, pp. 1308–1326, 2024.
- [21] Y. Xu, Y. Mao, O. Dizdar, and B. Clerckx, "Rate-Splitting Multiple Access With Finite Blocklength for Short-Packet and Low-Latency Downlink Communications," *IEEE Trans. Veh. Technol.*, vol. 71, no. 11, pp. 12 333–12 337, 2022.
- [22] S. Pala, M. Katwe, K. Singh, B. Clerckx, and C.-P. Li, "Spectral-Efficient RIS-Aided RSMA URLLC: Toward Mobile Broadband Reliable Low Latency Communication (mBRLC) System," *IEEE Trans. Wireless Commun.*, vol. 23, no. 4, pp. 3507–3524, 2024.
- [23] O. Dizdar, Y. Mao, and B. Clerckx, "Rate-Splitting Multiple Access to Mitigate the Curse of Mobility in (Massive) MIMO Networks," *IEEE Trans. Commun. Technol.*, vol. 69, no. 10, pp. 6765–6780, 2021.
- [24] R.-J. Reifert, S. Roth, A. A. Ahmad, and A. Sezgin, "Comeback kid: Resilience for mixed-critical wireless network resource management," *IEEE Trans. Veh. Technol.*, vol. 72, no. 12, pp. 16 177–16 194, 2023.
- [25] H. Wang, Z. Han, and A. L. Swindlehurst, "Non-Diagonal RIS Empowered Channel Reciprocity Attacks on TDD-Based Wireless Systems," in *IEEE International Conference on Communications (ICC)*, 2024, pp. 127–132.
- [26] H. Huang, H. Zhang, J. Yuan, L. Sun, Y. Wang, W. Mei, B. Di, Y. Cai, and Z. Han, "Disco Intelligent Omni-Surfaces: 360-degree Fully-Passive Jamming Attacks," *arXiv preprint arXiv:2411.12985*, 2024.
- [27] A. Konar and N. D. Sidiropoulos, "Fast approximation algorithms for a class of non-convex QCQP problems using first-order methods," *IEEE Trans. Signal Process.*, vol. 65, no. 13, pp. 3494–3509, 2017.
- [28] L. Dieci, A. Papini, and A. Pugliese, "Takagi Factorization of Matrices Depending on Parameters and Locating Degeneracies of Singular Values," *SIAM Journal on Matrix Analysis and Applications*, vol. 43, no. 3, pp. 1148–1161, 2022.
- [29] J. R. Magnus and H. Neudecker, "The Elimination Matrix: Some Lemmas and Applications," *SIAM Journal on Algebraic Discrete Methods*, vol. 1, no. 4, pp. 422–449, 1980.